Effect of Air Exposure on Surface Properties, Electronic Structure, and Carrier Relaxation in PbSe Nanocrystals

Milan Sykora,[†,*] Alexey Y. Koposov,[†] John A. McGuire,[†,§] Roland K. Schulze,[‡] Olexandr Tretiak,[†] Jeffrey M. Pietryga,[†] and Victor I. Klimov[†,*]

[†]Center for Advanced Solar Photophysics, Chemistry Division, Los Alamos National Laboratory, Los Alamos, New Mexico 87545, [‡]Materials ScienceDivision, Los Alamos National Laboratory, Los Alamos, New Mexico 87545, and [§]Present address: Department of Physics and Astronomy, Michigan State University, East Lansing, Michigan 48824

ABSTRACT Effects of air exposure on surface properties, electronic structure, and carrier relaxation dynamics in colloidal PbSe nanocrystals (NCs) were studied using X-ray photoelectron spectroscopy, transmission electron microscopy, and steady-state and time-resolved photoluminescence (PL) spectroscopies. We show that exposure of NC hexane solutions to air under ambient conditions leads to rapid oxidation of NCs such that up to 50% of their volume is transformed into PbO, SeO_2, or $PbSeO_3$ within 24 h. The oxidation is a thermally activated process, spontaneous at room temperature. The oxidation-induced reduction in the size of the PbSe "core" increases quantum confinement, causing shifts of the PL band and the absorption onset to higher energies. The exposure of NC solutions to air also causes rapid (within minutes) quenching of PL intensity followed by slow (within hours) recovery during which the PL quantum yield can reach values exceeding those observed prior to the air exposure. The short-term PL quenching is attributed to enhanced carrier trapping induced by adsorption of oxygen onto the NC surface, while the PL recovery at longer times is predominantly due to reduction in the efficiency of the "intrinsic" nonradiative interband recombination caused by the increase of the band gap in oxidized NCs. Although the analysis of subnanosecond relaxation dynamics in air-exposed NCs is complicated by a significant enhancement in fast carrier trapping, our picosecond PL measurements suggest that air exposure likely has only a weak effect on Auger recombination and also does not significantly affect the efficiency of carrier multiplication. We also show that the effects of air exposure are partially suppressed in PbSe/CdSe core/shell structures.

KEYWORDS: PbSe · nanocrystals · quantum dots · photochemistry · Auger recombination · carrier multiplication · multiexciton generation

The development of wet-chemistry synthetic routes for the fabrication of high-quality lead chalcogenide (PbS, PbSe, and PbTe) nanocrystals (NCs)[1−6] created an opportunity for exploitation of these materials in practical applications where the tunability of electronic properties in the near-infrared (NIR) region of the optical spectrum is of particular importance. Recent demonstrations of amplified spontaneous emission[7] and electroluminescence[8,9] as well as the development of solution-processable field effect transistors[10] and solar cells[11−14] using lead chalcogenide NCs have shown that these materials have great potential to enable new or enhance existing technologies. One potential obstacle to broad application of lead chalcogenide NCs is their limited chemical and photochemical stability. For example, observation of amplified spontaneous emission from PbSe NCs typically requires incorporation of the NCs into a sol−gel matrix to protect them from photodegradation.[7] In studies of PbSe NC-based field effect transistors and solar cells it was shown that under ambient conditions the semiconducting NC films rapidly degrade into highly conductive p-type solids, which is detrimental to the performance of the devices.[10,15]

Recent optical and X-ray photoelectron spectroscopy (XPS) studies of air-exposed PbS and PbSe NC films provided convincing evidence that under aerobic conditions the dominant degradation mechanism is surface oxidation of the NCs by atmospheric O_2.[15−19] Dramatic spectral shifts observed in steady state absorption and photoluminescence (PL) revealed that surface oxidation induces significant changes in the electronic structure of the NCs, related primarily to the reduction in their size.[16,17] While the origins of the spectral shifts in the air-exposed films are now understood, a systematic study of PbSe NCs in air-exposed solutions has been lacking, and the effects of air exposure on carrier relaxation processes in NCs are still largely unexplored.

Understanding carrier relaxation processes in NCs is essential for a number of potential applications. For example, optical amplification in NCs depends strongly on the efficiency of nonradiative relaxation processes, such as Auger recombination and surface trapping.[7,20,21] The ability to control relaxation pathways in NCs is also critical for photovoltaic applications. One process that has been extensively studied

*Address correspondence to sykoram@lanl.gov, klimov@lanl.gov.

Received for review January 21, 2010 and accepted March 26, 2010.

Published online April 6, 2010. 10.1021/nn100131w

in this context is carrier multiplication (CM), whereby multiple excitons are generated following absorption of a single photon.[22−27] Successful exploitation of CM in practical technologies is strongly dependent on our ability to eliminate or minimize competing relaxation processes.[28] In recent theoretical[29] and experimental[30,31] studies it was suggested that changes in the surface properties of NCs have a pronounced effect on the rate of nonradiative relaxation and can also potentially affect the efficiency of the CM process.

In the present work, we analyze the effect of air exposure on surface chemical composition, optical properties, and carrier relaxation dynamics in PbSe NCs suspended in hexane. Our studies of carrier relaxation dynamics on microsecond and subnanosecond time scales reveal that dramatic variations in the PL quantum yield (QY), observed following air exposure, can be explained in terms of changes in the efficiencies of two relaxation processes: carrier surface trapping and "intrinsic" nonradiative interband recombination controlled by the width of the NC band gap. Enhancement of surface trapping in air-exposed NCs can lead to difficulties in the accurate determination of Auger recombination rates and overestimations of CM efficiencies. However, after accounting for enhanced carrier trapping and oxidation-induced reduction in the NC core size, we demonstrate that the dramatic changes in the surface properties of oxidized NCs have only a weak effect on Auger decay and do not significantly affect the efficiency of CM. Finally, we show that the effects of air exposure can be reduced (but not completely eliminated) if PbSe NCs are protected by a thin shell of CdSe produced *via* an ion exchange process.[6]

RESULTS AND DISCUSSION

Effect of Air Exposure on Absorption and Steady-State PL Spectra. In previous studies of PbSe and PbS NC films[16,17] it was shown that exposure of NC films to air at ambient conditions leads to dramatic changes in their absorption and PL spectra. Differences in the PL spectra of freshly prepared air-exposed tetrachloroethylene solution of PbSe NCs and the same solution stored for 1−2 months were also reported.[16,17] To quantitatively understand the effect of air exposure on electronic properties of PbSe NCs in solution, we monitored short and long-term changes in absorption and PL spectra for a series of samples of various NC sizes prepared as hexane solutions and stored under air-free (argon atmosphere, sealed cuvettes) and air-exposed (atmospheric pressure, open cuvettes) conditions.

Figure 1 shows changes in the absorption and PL spectra observed for PbSe NCs with initial energy gap $E_g = 0.61$ eV (particle diameter $d \approx 7.6$ nm)[32] during exposure to air. Within minutes, a significant blue shift and broadening of the absorption features and the PL band were observed. After 24 h, the PL band shifted by ~160 meV to higher energies and the band full-width

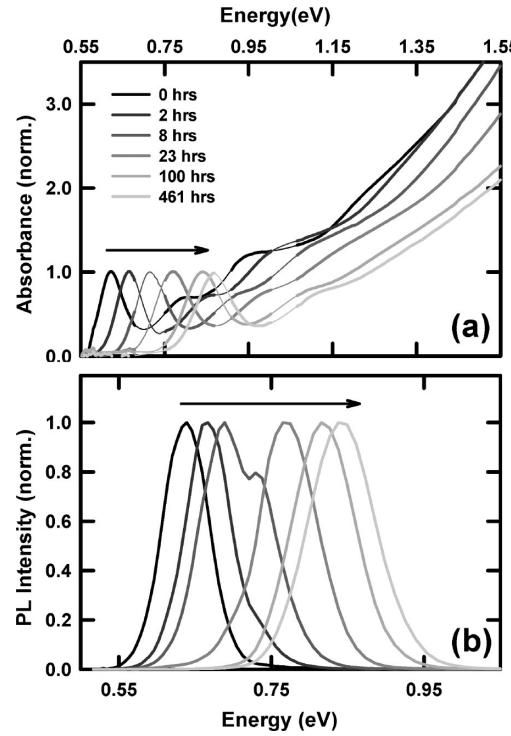

Figure 1. (a) Evolution of absorption spectra of PbSe NCs (initial gap $E_g = 0.61$ eV) dissolved in hexane upon exposure to air at room temperature. The NC solution was kept in the dark between measurements. The thin sections of the traces are interpolations in regions where the spectrum was distorted by solvent. (b) Evolution of PL spectra for the same sample. The excitation photon energy is 1.54 eV.

at half-maximum (fwhm) increased from 61 to 86 meV. The rate of the shift of the mean PL band energy ($\langle E \rangle = \int EI(E)\,dE / \int I(E)\,dE$), where $I(E)$ is PL intensity at energy E), gradually slowed from an initial value of ~30 meV per hour to less than 0.2 meV per hour after 100 h.

A summary of the observed changes in the mean PL band energy for a series of NCs of various sizes, under air-free and air-exposed conditions and room-light illumination is shown in Figure 2 panels a and b, respectively. Also included are the data for PbSe/CdSe core/shell structures (sample D). Under air-free conditions and ambient irradiation (Figure 2a), the mean PL band energy remained constant for all studied samples for more than a month. In contrast, all air-exposed samples except for core/shell NCs showed a continuous blue shift of the PL band, which became apparent within the first few minutes of air exposure (Figure 2b). In all cases, the PL band continuously shifted for the entire duration of the experiment, which lasted 6 weeks. While we have not observed systematic variations in the dynamics or magnitude of the shifts with NC size, we have noticed sensitivity to slight variations in the synthetic procedure. For example, for two batches of PbSe NCs with $E_g = 0.61$ eV ($d \approx 7.6$ nm) prepared following a nominally identical procedure, we observed differences in the rate of the PL band shift of about a factor of 4. When comparing sensitivity to light exposure, we have not seen any apparent differences between NCs stored

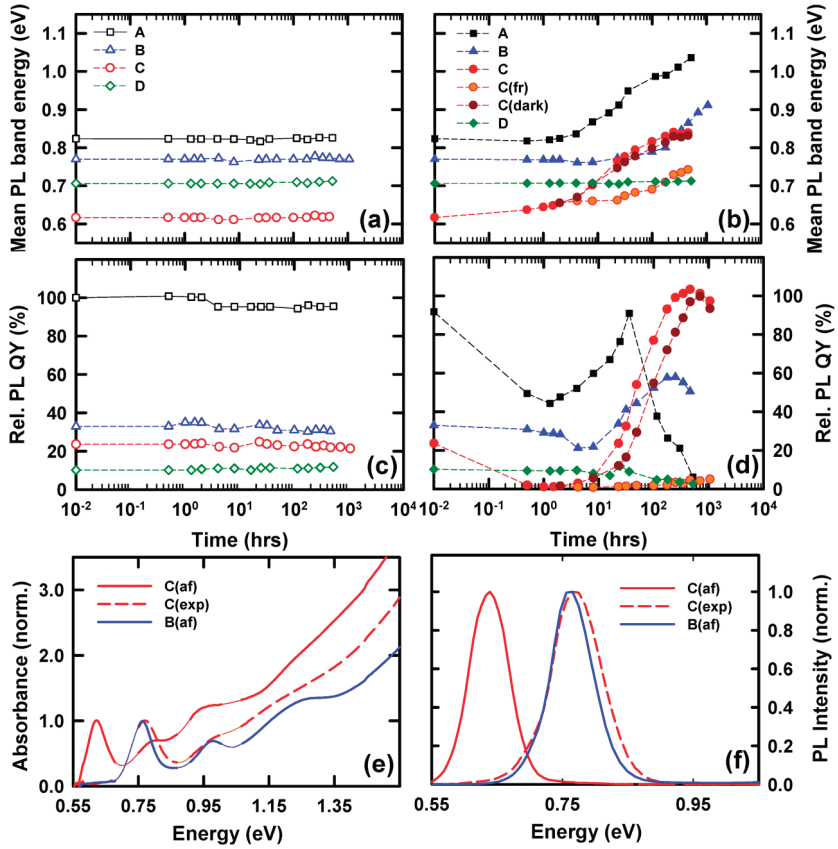

Figure 2. (a) Variations in the PL band energy measured as a function of time for three sizes of PbSe NCs (A−C) and PbSe/CdSe core/shell NCs (D) in hexane, stored under argon in sealed cuvettes at room temperature and under ambient light. (b) Variations in the PL band energy for the same series of samples during exposure to air. Also included are the data for sample C stored in the dark at room temperature (labeled "dark") and at −35 °C (labeled "fr"). (c) Variations in the PL quantum yields for the same series of samples as in panel a. (d) Variations in the PL quantum yields for the samples shown in panel b. Because of the uncertainty in the error associated with the PL QY of the reference dye IR26, the PL QYs are shown as relative values, normalized with respect to the initial PL QY of sample A under air-free conditions (this sample shows a PL QY of ~100% relative to IR26). (e) Comparison of the absorption spectra of the NCs with E_g = 0.61 eV under air-free conditions (C(af)) and after exposure to air for ~24 h (C(exp)) with the absorption spectrum of independently prepared NCs with E_g = 0.77 eV and measured under air-free conditions (B(af)). The thin line segments of the traces indicate regions where the absorption of the NCs is distorted by the absorption features of the solvent. (f) The PL spectra for the same series of samples as in panel e.

under ambient light or in the dark (sample C(dark) in Figure 2b). Interestingly, the PL band shift slowed significantly at reduced temperatures (see sample C(fr) in Figure 2b, stored at temperature −35 °C).

We also monitored changes in the PL QY induced by air exposure (Figure 2c,d). The PL QY of NCs was measured against the IR emitting organic dye, IR26 (Exciton), in 1,2-dichloroethane as a reference, assuming that the dye emission efficiency was 0.50%.[33,34] The results summarized in Figure 2c (same samples as in Figure 2a) show that the PL QY of air-free samples remained constant for the duration of the experiment. We have also noticed that with the exception of the core/shell structures, the PL QY of air-free samples showed a systematic decrease with decreasing E_g (increasing NC size). During air exposure (Figure 2d, same samples as in Figure 2b), the PL QY dropped rapidly for all PbSe samples, and in some cases the PL was completely quenched. However, after the initial drop, the PL typically recovered within the next few hours, and the QY eventually exceeded the value observed prior to air-exposure. After several days to weeks (depending on sample) the PL gradually decreased again and in some cases disappeared irrecoverably. The storage of samples in the dark did not have a significant effect on the rate of PL recovery (see samples C and C(dark) in Figure 2d). However, when NCs were stored in a freezer (temperature −35 °C), the rate of PL recovery was significantly slower (C(fr), Figure 2d).

It is important to note that the rate and the magnitude of PL QY variations during air exposure were sensitive to small changes in the synthetic procedure. For example, if the heating of the reaction mixture prior to the injection of trioctylphosphine selenium (TOPSe) was done under static argon atmosphere rather than under continuous argon flow (see Methods) or the di-*i*-butylphosphine was added to the cold reaction mixture after the reaction step involving the argon flow was complete, the exposure to air of the produced NCs resulted in an irrecoverable loss of PL on a time scale of

several hours. We attribute this effect to a difference in the amounts of volatile di-*i*-butylphosphine which is present in the reaction mixture at the point of the TOPSe injection in the case of static inert atmosphere *versus* the situation of the continuous argon flow. We hypothesize that a small amount of di-*i*-butylphosphine either affects the surface chemical composition of the NCs (*i.e.*, Pb/Se ratio)[35] or, as a surface ligand, directly interferes with the surface oxidation process, significantly enhancing the efficiency of carrier trapping. The interplay between different factors that affect PL QY is discussed later in this section.

In Figure 2e,f, we compare the PL and absorption spectra of the air-exposed NCs with those of the NCs of the same energy gap but prepared and stored under argon atmosphere. This comparison shows that, while the spectral features of the two samples are similar, the peaks are noticeably broader for the air-exposed sample, suggesting larger NC size dispersion.

Our observation of air-exposure-induced PL quenching on a time scale of less than a few hours is consistent with previous reports of rapid PL quenching of air-exposed PbS and PbSe NC films on glass or Si substrates.[16,17] These earlier studies demonstrated that the initial fast drop in the PL intensity is not due to atmospheric water vapor but rather is caused by reversible physisorption of O_2 onto the NC surface. While the exact mechanism of PL quenching was not identified, it was suggested that it was either due to a direct interaction of a photogenerated exciton with surface adsorbed O_2 or due to an O_2-induced modification of the NC surface properties, such as surface charging.[17]

To test the reversibility of PL quenching in our PbSe NC solutions, we purged the samples briefly exposed to air with argon gas. We found that even if the PL is initially completely quenched, it could be almost fully recovered in the purged samples. No shift of the PL band was observed before or after purging. On the basis of this result, we conclude that the initial drop in PL QY observed in the PbSe NC solutions is due to the same O_2 surface adsorption process as the one previously observed in NC films.[16,17] The difference in the rate of PL QY drop is possibly due to a significant difference in mole fractions of O_2 in air and *n*-hexane (at 298 K, $x_{air}^{O_2} = 0.21$, $x_{n\text{-hexane}}^{O_2} = 2.0 \times 10^{-3}$).[36,37]

To gain further insights into the mechanism of the short-term PL quenching, we monitored the evolution of the nanosecond PL dynamics of the NCs with $E_g = 0.81$ eV ($d \approx 5.0$ nm) for the first 4 h of air exposure. The results are summarized in Figure 3a. Over the studied period, we observed a drop of ~50% in the overall PL intensity obtained by integrating the area under the nanosecond PL dynamics trace (consistent with the drop in PL QY), but no apparent change in the relaxation dynamics could be detected within the temporal resolution of ~1 ns used in these measurements. All decays could be fit to a single-exponential relaxation function, yielding a similar lifetime of ~200 ns. This result indicates that the adsorption of O_2 onto the PbSe NC surfaces leads to quenching of excitons on subnanosecond time scales, unresolvable in this experiment. Our attempt to study the PL relaxation with subnanosecond time resolution using PL upconversion (uPL) was unsuccessful because of the long acquisition times (>12 h) typically required to achieve a sufficiently high signal-to-noise ratio in these measurements. However, as discussed in later sections, in samples exposed to air for ~24 h we were able to detect a new relaxation channel with a time constant of ~100 ps that we tentatively attribute to the presence of O_2 adsorbed on NC surfaces.

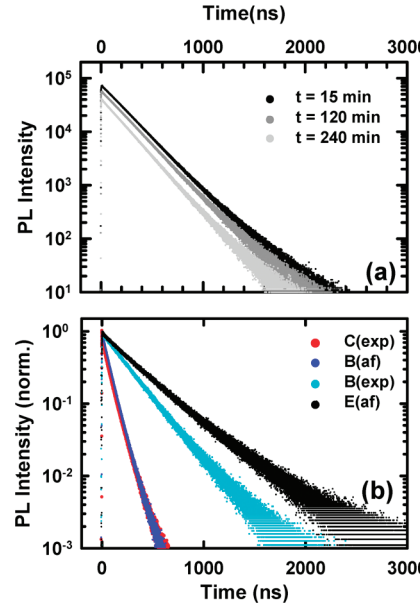

Figure 3. (a) Changes in the nanosecond PL relaxation dynamics for NCs with $E_g = 0.81$ eV monitored at the PL peak during the first 4 h of air exposure. (b) PL dynamics for NCs with initial $E_g = 0.61$ eV recorded after ~24 h of air exposure resulting in a PL peak of 0.77 eV (C(exp)) and independently prepared NCs with $E_g = 0.77$ eV stored and measured under air-free conditions (B(af)) (these two samples show nearly overlapping traces) and after ~500 h of air exposure monitored at the PL peak at 0.90 eV (B(exp)). Also shown is the PL dynamics of independently prepared NCs with $E_g = 1.0$ eV stored and measured under air-free conditions (E(af)).

The recovery of the PL intensity observed for NC solutions on a time scale of a few hours (Figure 2d) is in contrast to previous observations of an irrecoverable loss of PL in PbS films.[16] Stouwdam *et al.*[17] suggested that in small PbS NCs ($E_g = 1.2-1.3$ eV) this effect is due to efficient quenching of NC excitons by a highly reactive singlet O_2 ($a^1\Delta_g$) state with an energy of ~0.98 eV. This process is not expected to be efficient for the larger PbSe NCs studied here ($E_g = 0.61-0.81$ eV). On the other hand, it is interesting to note that for the smallest NCs (sample A), with initial $E_g = 0.81$ eV, we observed a dramatic drop in the PL QY in the air-exposed sample when the NC energy gap shifted to 0.97−0.98

eV (see Figure 2b,d). This observation is consistent with the mechanism proposed in ref 17.

One important observation is that the beginning of the PL QY recovery correlates with the onset of the blue shift of the PL and the absorption spectra, indicating that these changes may relate to the changes in the band gap of the air-exposed NCs. This assessment is supported by studies of nanosecond PL dynamics for series of air-free and air-exposed samples (Figure 3b). Interestingly, the relaxation dynamics of the air-free sample (labeled B(af); NC $E_g = 0.77$ eV) and the air-exposed sample with the same energy gap (labeled C(exp) and obtained by ~24 h of air exposure of the NCs with an initial energy gap of 0.61 eV) are nearly identical with an exciton lifetime (τ) of ~75 ns. This suggests that on nanosecond time scale the exciton recombination dynamics is insensitive to the changes in NC surface properties induced by air exposure, but is controlled primarily by the width of the energy gap (or size) of the PbSe NCs. Another interesting observation is that when the air-free sample, B(af), is exposed to air for ~500 h (B(exp)) the exciton lifetime increases by approximately a factor of 3 to ~246 ns, which is accompanied by a shift in the PL band from 0.77 to 0.90 eV and QY increase from ~35% to ~62%. Assuming a direct correlation between the energy gap and the exciton lifetime, one would expect a further increase in τ with increasing E_g. Indeed, we observed an even longer exciton lifetime ($\tau \approx 341$ ns) for NCs with $E_g = 1.0$ eV (E(af) in Figure 3b) prepared under air-free conditions. This result is consistent with recent observations of the size-dependence of exciton lifetimes in PbSe[38,39] and PbS[39,40] NCs. All of these results suggest that the increase in PL QY observed in air-exposed samples on time scales of several hours (Figure 2d), can be at least in part attributed to the dependence of the recombination dynamics on NC size.

The exciton decay is due to both radiative (decay rate k_r) and nonradiative processes (decay rate k_{nr}). The nonradiative losses can be further separated into ones due to surface trapping (rate k_t) and those due to "intrinsic" radiationless interband recombination (rate k_i): $k_{nr} = k_t + k_i$. Taking into account all of these recombination pathways, the exciton lifetime, τ, and PL QY can be expressed as $1/\tau = k_r + k_t + k_i$, and $QY = k_r/(k_r + k_t + k_i)$, respectively.

Within the particle-in-a-box model, the radiative decay rate does not significantly vary with NC size and is primarily determined by the bulk-semiconductor emission dipole corrected for dielectric screening effects.[41] Therefore, the observed increase in the exciton lifetime and a complementary growth of PL QY are likely associated with changes in the rates of nonradiative processes. As discussed above for the case of surface-adsorbed oxygen and also indicated by ultrafast PL studies discussed below, carrier trapping at surface defects formed as a result of surface oxidation is characterized by fast subnanosecond dynamics. These dynamics are unresolved in the above measurements, which have ~1 ns resolution. In contrast, as suggested by the similarity of dynamics for air-free and air-exposed samples with the same gap show in Figure 3, the observed modification in PL dynamics that involves the submicrosecond time scale are most likely indicative of changes in "intrinsic" nonradiative decay channels characterized by the rate k_i.

A recent study of carrier cooling dynamics in PbSe NCs discussed the role of intrinsic phonon-related processes in intraband carrier relaxation.[42] Specifically, multiphonon emission mediated by nonadiabatic electron−phonon interactions was invoked to explain the size-dependence of the measured intraband energy losses.[42] We hypothesize that a similar multiphonon nonradiative decay process contributes to interband exciton recombination. The efficiency of multiphonon transitions is expected to rapidly decrease with increasing E_g,[43] which may explain the increase in the exciton lifetimes accompanied by the growth of PL QY observed during the increase in the NC energy gap associated with oxidation of the NCs (Figures 2b,d). Multiphonon emission underlies the effect known as the "energy gap law",[44] well-known for molecular systems where it is used to explain the decrease in the rate of nonradiative relaxation with increasing energy gap. A similar mechanism has been used to explain nonradiative recombination involving defect states in solids.[45]

To summarize, the effect of surface oxidation on carrier dynamics is 2-fold. The oxidation-induced formation of surface defects leads to increased nonradiative losses due to enhanced surface trapping. On the other hand, the widening of the energy gap as a result of the decreasing size of the PbSe core leads to suppression of the "intrinsic" nonradiative recombination that we tentatively assign to multiphonon interband transitions. The outcome of these two competing trends likely depends on the exact composition of the NC interface and may differ from sample to sample depending on variations (possibly uncontrolled) in synthetic procedures. In the case of samples in Figure 2, the suppression of "intrinsic" nonradiative recombination due to increasing E_g dominates over additional carrier losses induced by enhanced surface trapping. Therefore, the net effect of surface oxidation is an increase in the PL QY. However, in some of the samples (*e.g.*, those fabricated using heating under static argon atmosphere; see above), the long-term PL recovery is not observed indicating the overwhelming role of additional relaxation pathways associated with surface defects formed as a result of NC oxidation.

Effects of Air Exposure on NC Surface Composition and NC Size. To understand the effect of air exposure on chemical composition of the NCs, we performed comparative XPS studies of air-free and air-exposed samples. Figure 4 summarizes the results of this study for NCs with

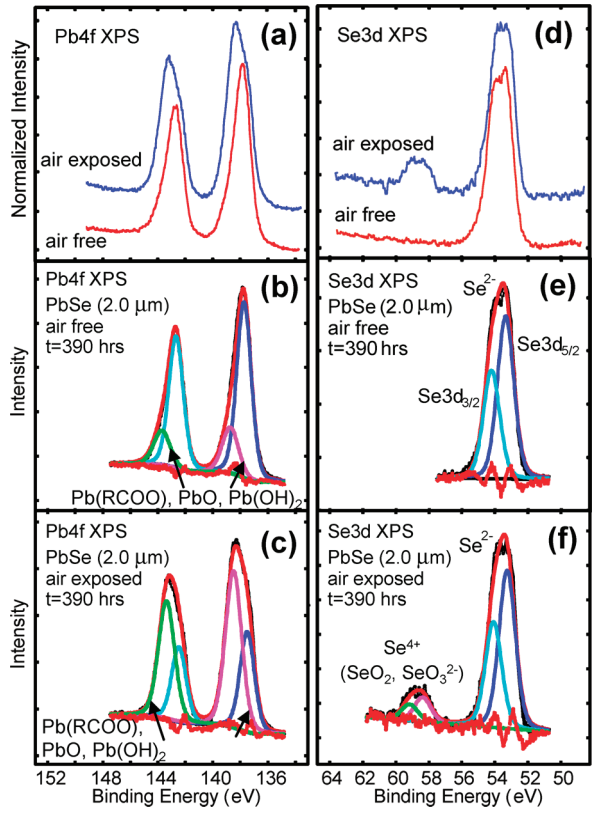

Figure 4. XPS analysis of PbSe NCs (E_g = 0.61 eV) stored under air-free conditions and air exposed in hexane solution for 390 h (E_g = 0.77 eV). Panels a and d show comparison of the raw data in the Pb(4f) and in the Se(3d) regions. Panels b,c and e,f show the results of the spectral curve fitting in the two regions showing the relative contributions of chemical states due to various metal components that are present at the surfaces of the NCs. Binding energies of the various fit component peaks are restricted to the known energies of the chemical states present.

initial energy gap E_g = 0.61 eV ($d \approx$ 7.6 nm). The XPS spectra of the air-exposed sample were collected following ~390 h of air exposure. According to the optical studies (Figure 2b,d), the air-exposed sample had at the time of the XPS measurement $E_g \approx$ 0.84 eV and PL QY of ~100%.

The XPS spectrum in the range of 136 to 148 eV (Figure 4a) is dominated by two features at ~138 and ~143 eV that arise from the $4f_{5/2}$ and $4f_{7/2}$ spin−orbit coupled doublet of Pb. An analysis of XPS spectra (Figure 4b,c) indicates that the doublet cannot be satisfactorily modeled in terms of a single Pb species and that at least two types of Pb^{2+} are present in the NCs. These different chemical states are resolved through curve fitting. We attribute the lower-energy feature in each band of the doublet (137 and 142.5 eV) to the Pb^{2+} ions in PbSe. Because of a higher binding energy of Pb−O compared to Pb−Se, the higher-energy features (138 and 143.5 eV) are assigned to Pb−O adducts in the form of lead oleate, $Pb(OOCR)_2$; lead oxide, PbO; lead hydroxide, $Pb(OH)_2$; or their combination. In the air-free sample, we attribute the high-energy features to the surface Pb^{2+} ions bound to oleic acid. As evident from Figure 4 panels a and c, the high-energy feature is significantly enhanced in the air-exposed sample indicating a significantly higher amount of Pb−O adducts. A similar enhancement of Pb 4f features was previously observed in air-exposed PbSe films and attributed to formation of lead oxides or hydroxides.[15]

We have also observed clear signatures of selenium oxidation in the air-exposed sample in the region of the Se 3d core line at 50 to 62 eV. The spectrum in this range is dominated by the signal of the Se^{2-} 3d core level at 54.6 eV, which is broadened due to the presence of two Se features, corresponding to $3d_{5/2}$ and $3d_{3/2}$ levels. While there is no apparent shape change in the main feature, when comparing the air-free and air-exposed samples, a new feature appears in the air-exposed sample at ~59 eV. The analysis of this feature (Figure 4e,f) shows that it can be modeled by two bands with separation identical to the splitting of the $3d_{5/2}$ and $3d_{3/2}$ components in the main band (~0.9 eV), with a 6:4 ratio of the band intensities as expected according to the states' degeneracies. This indicates that the new feature is associated with a different oxidation state of Se, attributed to Se^{4+}, most likely in the form of SeO_3^{2-} or SeO_2. Our observations are consistent with previous XPS studies of air-exposed bulk PbSe,[46] chemical-bath-deposited PbSe films,[47] previous synchrotron photoelectron spectroscopy studies of PbSe NCs,[48] and more recent studies of 1,2 ethanedithiol-treated PbSe NC films.[15]

In Figure 5, we compare TEM images of PbSe NCs with initial energy gaps E_g = 0.61 eV and E_g = 0.77 eV either stored under air-free conditions or air exposed in hexane solution for ~390 h. As apparent from these images and the histograms (shown as insets), air exposure leads to a dramatic increase in NC size dispersion and a decrease in the average PbSe core size. The reduction of the average size is especially dramatic for larger NCs. For example, for particles with an initial diameter of ~7.6 nm, the average size decreased by almost 3 nm over ~3 weeks of air exposure (Figure 5a,b). Over the same period of time the PL blue-shifted by ~0.25 eV (0.61−0.86 eV), which correlates well with the observed change in size.[32] This reduction in NC size is more significant than the previously reported ~0.5 nm change observed upon 2 months of air exposure of PbSe NCs in CCl_4.[49] However, the NCs used in ref 49 (E_g = 0.86 eV) are closer in size to the smaller NCs studied here (E_g = 0.77 eV), for which the change in average diameter was ~1 nm (Figure 5c,d).[50]

The apparent increase in size dispersion in both samples explains the observed broadening of spectral features in absorption and PL spectra (Figure 2e,f). The increase in polydispersity is likely a result of a nonuniform rate of NC oxidation. In addition, as was shown in a recent nuclear magnetic resonance (NMR) study by Moreels *et al.*,[49] surface oxidation of PbSe NCs can cause a significant loss of surface Pb atoms and up to 30% loss of surface ligands, which leads to significant

aggregation and precipitation of NCs. Consistent with this report, in our TEM images of air-exposed samples, we detected significant amounts of large particle aggregates with sizes well above 20 nm, most likely responsible for the observed precipitation. No precipitation or aggregation was observed in the air-free samples.

Oxidation Chemistry of PbSe NCs. One important question is that of the chemical composition of the PbSe oxidation products. Thermodynamic considerations suggest that under ambient conditions, the oxidation process can proceed through a number of pathways as shown, with compound oxides likely to dominate the product mix.[51]

$$PbSe(s) + 2O_2(g) \rightarrow PbSeO_4(s) \qquad \Delta G^0_{298} = -405 \text{ kJ/mol} \quad (1)$$

$$PbSe(s) + 3/2O_2(g) \rightarrow PbSeO_3(s) \qquad \Delta G^0_{298} = -352 \text{ kJ/mol} \quad (2)$$

$$PbSe(s) + 3/2O_2(g) \rightarrow PbO(s) + SeO_2(s) \qquad \Delta G^0_{298} = -262 \text{ kJ/mol} \quad (3)$$

$$PbSe(s) + 1/2O_2(g) \rightarrow PbO(s) + 1/2Se_2(s) \qquad \Delta G^0_{298} = -201 \text{ kJ/mol} \quad (4)$$

$$PbSe(s) + O_2(g) \rightarrow Pb(s) + SeO_2(s) \qquad \Delta G^0_{298} = -74 \text{ kJ/mol} \quad (5)$$

$$PbSe(s) + O_2(g) \rightarrow PbO(s) + SeO(g) \qquad \Delta G^0_{298} = -64 \text{ kJ/mol} \quad (6)$$

While comparison of equilibrium free energies for processes (1) to (6) implies that $PbSeO_4$ is thermodynamically the most favorable product, experimental studies of bulk PbSe oxidation have shown that the mix of products formed on the semiconductor surface is dominated by SeO_2, PbO, and $PbSeO_3$.[46,51−53] This implies that reaction 1 is kinetically inhibited at room temperature. Our observations of a pronounced Se^{4+} peak and an increase in the amount of Pb−O adducts in the XPS spectra of the air-exposed PbSe NCs strongly suggest that the oxidation of the NCs in solution proceeds in a way similar to bulk, most likely *via* a combination of reactions 2 to 4.[54] Because of the similarities in electron densities on Pb and Se atoms in simple oxides (PbO, SeO_2) and $PbSeO_3$, the determination of the relative amounts of these oxides solely based on the XPS data is difficult. However, in previous studies of CdSe NCs it was shown that SeO_2 formed as a result of air exposure desorbs from NC surfaces under ambient conditions.[55] Assuming that SeO_2 is equally prone to desorption on PbSe NC surfaces, our observation of a strong Se^{4+} signature in the XPS spectra of all studied PbSe NCs suggests that at least a fraction of the NC surfaces is in the form of the more stable compound oxide, $PbSeO_3$.

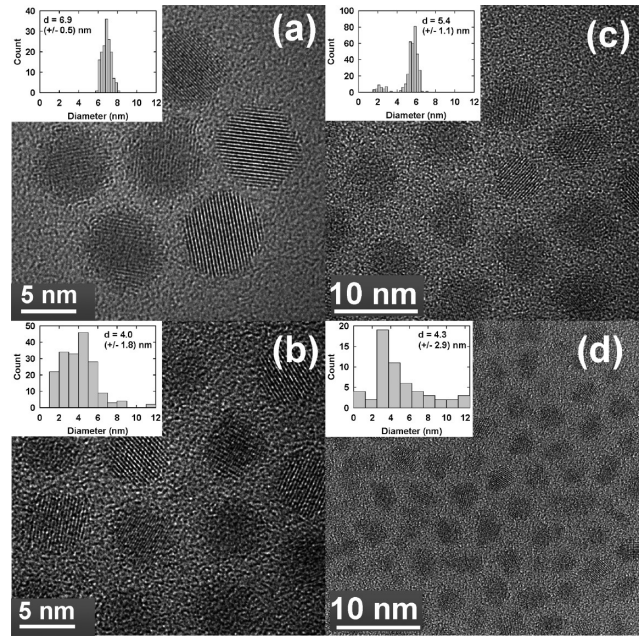

Figure 5. (a) TEM images of PbSe NCs with initial E_g = 0.61 eV stored under air-free conditions. (b) The same NCs as in panel a but after air exposure in hexane solution for 390 h. (c) PbSe NCs (initial E_g = 0.77 eV) stored under air-free conditions. (d) The same NCs as in panel c after air exposure in hexane solution for 390 h. The insets show the size-distribution histograms obtained from the TEM images of more than 100 NCs.

It is also interesting to note that the free energy of processes (1) to (6) becomes more negative with decreasing temperature,[51] which means that the efficiency of oxidation should increase with decreasing temperature. This, however, is in contrast with our observations (see Figure 2b,d), which clearly show that the rate of NC oxidation is dramatically reduced for samples stored at −35 °C. This result implies that oxidation is controlled not by equilibrium thermodynamics but rather by kinetic factors and involves a small activation barrier (25 °C corresponds to ∼26 meV)

A quantitative comparison of the rate of oxidation of bulk and NC forms of PbSe is possible by contrasting results of previous X-ray diffraction studies of air-exposed bulk PbSe (particles of 0.5−3 μm diameter)[51] and our studies of PL spectral shifts in NCs (Figure 2b). Using this approach, we find that the rate of bulk PbSe oxidation is significantly higher (50 vol % per ∼25 min) than that of the air-exposed NCs in solution (50 vol % per ∼16 h; for NCs in 5−8 nm range). We attribute this difference in part to the lower concentration of O_2 in hexane compared to air and in part to a protective effect of the NC surface ligands. In NC films the rate of oxidation is expected to be strongly dependent on the film's macroscopic properties (*e.g.*, thickness, uniformity, *etc.*), as these factors dictate the rate and the efficiency of oxygen diffusion into the film. Another important factor is the NC surface treatment, which can affect the rate of oxygen adsorption as well as the oxidation kinetics.

Stouwdam *et al.*[17] have attempted to stabilize PbSe NCs with respect to oxidation by epitaxially growing ~1 nm shell of PbS onto the PbSe core. However, the observed shifts and the drop in the PL signal upon air exposure showed that the PbS shell does not effectively protect the PbSe core from oxidation. For the PbSe/CdSe core/shell structures prepared in this work by a previously described ion-exchange approach[6] (shell thickness ~1.2 nm), the absence of shifts in either the absorption or PL spectra in the case of air-exposed samples (Figure 2b) indicates that the CdSe shell provides significantly better protection of the PbSe core from oxidation. However, the drop in the PL QY observed following several days of air exposure (Figure 2d) indicates the emergence of a new relaxation channel. In the absence of detectable spectral shifts and changes in submicrosecond dynamics, we attribute the reduction in the PL intensity to the formation of trap sites on the surface of the CdSe shell accessible by photoexcited carriers in the PbSe core. Significant effects of air exposure (or "aging") on surface properties of CdSe NCs and subnanosecond carrier relaxation dynamics were reported by several authors.[55−59]

Effect of Air Exposure on Auger Recombination and Carrier Multiplication. In our studies we have also analyzed the effect of air exposure on multiexciton Auger recombination as well as multiexciton generation from single photons *via* CM. In addition to their fundamental interest, these processes are important from a technological perspective as Auger recombination controls the optical gain dynamics in NC lasing media,[20] while CM has been widely considered as a potential enabler of generation III photovoltaics.[60]

To address the question of how surface oxidation affects the efficiency of Auger decay as well as the efficiency of the CM process, in the present work we performed a comparative study of carrier relaxation dynamics in air-free and air-exposed NCs using ultrafast PL upconversion (uPL).[61] The results are summarized in Figure 6. The top two panels show PL relaxation dynamics of air-free (a) and air-exposed (b) NCs following 1.54 eV excitation at various pump fluences. While the energy gap at the time of study was the same for both samples, $E_g = 0.77$ eV, the energy gap of the sample in panel b prior to air exposure was $E_g = 0.61$ eV. An increase in the magnitude and rate of relaxation with pump fluence observed for both samples provides a clear signature of multiexciton recombination *via* the Auger process. However, there is a notable difference in the relaxation dynamics observed at low pump fluences. While the air-free NCs show "flat" dynamics, there is a ~50% drop in the PL intensity observed in the oxidized NCs within the first 600 ps. This rapid drop in PL intensity is attributed to carrier trapping at defect sites (traps) formed at the NC surface as a result of oxygen adsorption and/or surface oxidation.

To evaluate the effect of oxidation on the efficiency of the Auger process we compared the biexciton Auger lifetimes ($\tau_{2,AR}$) of the air-free and air-exposed samples. Extracting the biexciton Auger recombination rate in well passivated samples (*i.e.*, samples showing flat dynamics under low-fluence excitation with 1.5 eV photons) is straightforward. The uPL traces can be fit to a biexponential decay, in which the slower decay time corresponds to the Auger relaxation of biexcitons and the faster decay time (only observed at higher fluences) corresponds to Auger relaxation of triexcitons. By simultaneously fitting decays recorded at all pump fluences we obtain for the air-free samples $\tau_{2,AR} = 146 \pm 2$ ps and $\tau_{3,AR} = 23.4 \pm 0.2$ ps for the sample with $E_g = 0.61$ eV, $\tau_{2,AR} = 75 \pm 1$ ps and $\tau_{3,AR} = 13.2 \pm 0.2$ ps ($E_g = 0.77$ eV; Figure 6a), and $\tau_{2,AR} = 55 \pm 1$ ps and $\tau_{3,AR} = 9.0 \pm 0.2$ ps ($E_g = 0.925$ eV) (details of the fits are provided in the Supporting Information).

Extracting an accurate value of the biexciton Auger recombination rate in samples displaying trapping is more complicated because of the contributions to the observed PL decay from excitons and multiexcitons both with and without surface-trapped carriers as well as the trapping process itself. An analysis explicitly including all components potentially contributing to the observed PL leads to a complex model with significant uncertainties associated with the large number of parameters. To obtain an estimate of $\tau_{2,AR}$ and $\tau_{3,AR}$, here we use a simpler approach based on the analysis of the components of triexponential fits to the experimental decays. The results of the fits for $E_g = 0.77$ eV ($E_g = 0.61$ eV prior to air exposure; Figure 6b) and for $E_g = 0.925$ eV ($E_g = 0.77$ eV prior to air exposure) are summarized in the Supporting Information. We make several simplifying assumptions about the contributions of various components to the individual time constants obtained by the fits. The value of τ_1, distinctly different from the time scales observed in air-free samples with the same gap, is taken to be the time scale for trapping, while τ_3 is assumed to be dominated by the Auger relaxation of triexcitons, which decay much more rapidly than biexcitons. The intermediate decay time, τ_2, then has contributions from Auger recombination of biexcitons with and without surface trapped carriers and single excitons with surface trapped carriers. In the limit that the trapping rate is significantly slower than the rate of Auger recombination (*i.e.*, $\tau_{3,AR} < \tau_{2,AR} \ll \tau_{trap}$) or that only a small fraction of nanocrystals undergo trapping, τ_2 represents an estimate for $\tau_{2,AR}$. A more accurate estimate is possible if we recognize that the decay of neutral biexcitons and triexcitons that can undergo trapping can be described by the compound decay rates of $2/\tau_{trap} + 1/\tau_{2,AR}$ and $3/\tau_{trap} + 1/\tau_{3,AR}$, respectively. This yields an approximation for the Auger decay time of biexcitons that can undergo trapping of

$$\tau_{2,AR} \approx 1/(1/\tau_2 - 2/\tau_{trap}) = 1/(1/\tau_2 - 2/\tau_1)$$

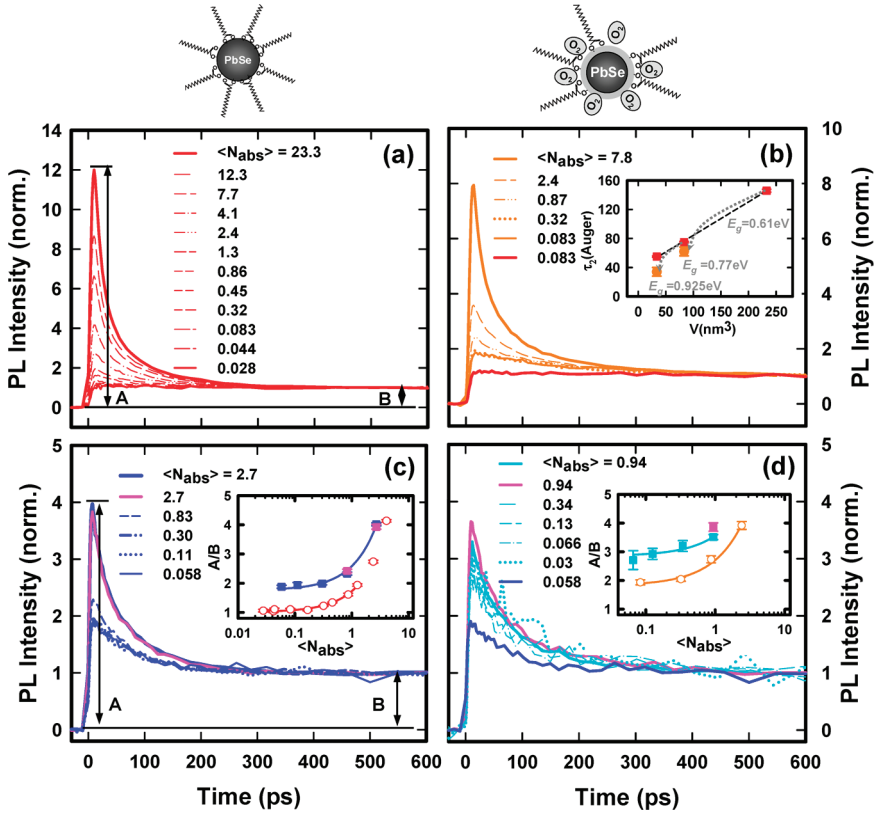

Figure 6. Time-resolved ultrafast photoluminescence (uPL) studies of NCs with E_g = 0.77 eV. (a) uPL traces for freshly prepared NCs stored and measured under air-free conditions in vigorously stirred hexane solution. The traces recorded for different pump intensities (indicated in the figure) are normalized at long time (>500 ps) after excitation; the excitation energy is 1.54 eV. (b) uPL dynamics for NCs with initial E_g = 0.61 eV after ~24 h exposure to air (orange traces). The red trace is a low-pump-fluence trace for the sample shown in panel a. The excitation energy is 1.54 eV. Inset: biexciton Auger rates extracted from traces in panels a and b and other NC sizes as a function of estimated NC volume. Arrows indicate the air-exposure-induced shift in NC core volume from the corresponding air-free sample. (c) Same as panel a except the excitation used is 3.08 eV. The magenta trace shows dynamics recorded in static solution. Inset: the ratio of the short- to long-time signals (A/B) as a function of $\langle N_{abs}\rangle$ (symbols) for 1.54 eV (red circles) and 3.08 eV (blue squares) excitation. The magenta squares are ratios obtained for dynamics measured in a static solution. The curves are linear fits to low- and moderate-fluence data. (d) Same as in panel c for a stirred solution of the sample with initial E_g = 0.61 eV after ~24 h exposure to air (cyan traces) and for the same sample measured in a static solution (magenta trace) and low-pump-fluence dynamics of the sample from panel c (blue trace). Inset: the ratio of the short- to long-time signals (A/B) as a function of $\langle N_{abs}\rangle$ (symbols) for 1.54 eV (orange circles) and 3.08 eV (cyan squares) excitation. The magenta square is a ratio obtained for dynamics measured in static solution. The lines are linear fits to the experimental data. Close agreement in A/B ratios for static and stirred samples indicates very low levels of persistent photoinduced charging in the static samples.

Since the uPL data shown in the main panel of Figure 6b imply that only a fraction, f_{trap}, of the air-exposed nanocrystals undergo trapping, we estimate the neutral multiexciton Auger recombination rates by $1/\tau_{2,AR} = 1/\tau_2 - f_{trap}2/\tau_{trap}$ and $1/\tau_{3,AR} = 1/\tau_3 - f_{trap}3/\tau_{trap}$. Using this approximation we obtain $\tau_{2,AR}$ = 62 ± 6 ps and $\tau_{3,AR}$ = 11 ± 1 ps (E_g = 0.77 eV) and $\tau_{2,AR}$ = 34 ± 6 ps and $\tau_{3,AR}$ = 6.6 ± 3.3 ps (E_g = 0.925 eV). The results of this analysis, summarized for $\tau_{2,AR}$ in the inset of Figure 6b, suggest that the effect of surface oxidation on Auger recombination is weak as indicated by only moderate changes of $\tau_{2,AR}$ (reduced by *ca.* 10−50%) in the air-exposed samples compared to the values for the air-free samples with the same energy gap.

The bottom two panels in Figure 6 show the results of our studies of PL dynamics for both air-free (c) and air-exposed (d) NCs following 3.08 eV excitation. For both samples, the data clearly show fast relaxation dynamics, indicative of generation of multiexcitons, even at pump fluences corresponding to a number of absorbed photons per NC per pulse of significantly less than one ($\langle N_{abs}\rangle \ll 1$). In several previous studies we[22] and others[23−27] have shown that this observation is due to multiexciton generation *via* CM. In this process, the excess energy of an electron or a hole created by absorption of a high-energy photon is transferred to a valence-band electron resulting in formation of a second electron−hole pair. An accurate determination of the quantum efficiency (QE) of the photon-to-exciton conversion is of great importance because of the potential of CM to enhance the performance of NC-based photovoltaics.[62,63]

In the original report of the effect in PbSe NCs[22] it was shown that dynamic signatures of multiexcitons in the transient absorbance (TA) signal can be effectively used to determine the QE in NCs. More recently,[28] it was

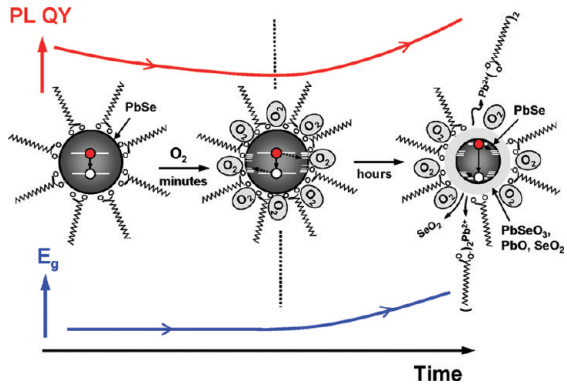

Scheme I. Effect of air exposure on surface composition and electronic and optical properties of PbSe NCs.

demonstrated that, after proper accounting for carrier thermalization, the analysis of ratios of early-to-late signal intensities (A/B) in TA and PL yields consistent values of QE. Using the approach developed in ref 28 and data in Figure 6c, we calculate the QE for the air-free sample to be QE(%) = 100(2 + A/B))/3 = 125 ± 5%, which corresponds to a biexciton yield of η_{xx} = 25% ± 5%. The analysis is more complicated in the case of air-exposed, oxidized samples where significant carrier trapping has a pronounced effect on the ratio of early-to-late PL intensities. As shown in the inset of Figure 6d, for a pump energy of 1.54 eV ($\eta\omega = 2.0E_g$), even at fluences significantly lower than those needed to generate multiexcitons directly by multiphoton absorption, the ratio of early-to-late signal intensities is significantly larger than one (A/B = 1.9 ± 0.1). Since carrier trapping is likely to have a similar effect on the data obtained with 3.08 eV pump, the equation used above to determine the CM QE in air-free samples will yield inflated apparent QEs. However, if the efficiency and dynamics of carrier trapping are assumed to be independent of the pump energy, it is possible to correct for the effect of trapping by utilizing low-pump-energy data and a modified expression for photon-to-exciton conversion efficiency; QE(%) = 100(2 + $(A/B)_{3.08}/(A/B)_{1.54}$).[64] Using this expression, for the air-exposed NCs we obtain QE = 119 ± 11% (η_{xx} = 19% ± 5%). This value is within the experimental error of the QE determined for the air-free sample. Our analysis of PL dynamics thus shows that the efficiency of the CM process is not significantly affected by the dramatic changes in surface properties of PbSe NCs induced by their exposure to air.

Model of PbSe NC Surface Oxidation. Using the results presented in the previous sections we propose the following model for describing the effect of surface oxidation on the optical properties of PbSe NCs (see Scheme I). During the initial stage of air exposure, rapid adsorption of oxygen onto the NC surface creates carrier surface traps that are responsible for the observed increase in the rate of PL relaxation and reduction in the PL QY. Following oxygen adsorption, thermal oxidation of PbSe is initiated, whereby surface Pb and Se atoms are converted into their respective oxides, PbO, SeO_2, or $PbSeO_3$. While SeO_2 is likely to desorb, at least a fraction of PbO and $PbSeO_3$ remains on the NC surface and can potentially form a thin shell around the PbSe core. According to results in ref 49 the oxidation is accompanied by irreversible loss of a fraction of Pb and oleic acid from the NC surface, which is likely the cause of NC aggregation. Based on ref 65 the band gap of $PbSeO_3$ is ~1.6 eV, which is much greater than the band gap of the PbSe core. The formation of the oxide could therefore be expected to have a passivating effect, reducing the efficiency of surface carrier trapping. However, results of our ultrafast PL studies clearly show enhanced nonradiative carrier trapping in oxidized NCs. Thus, while the surface oxidation of NCs provides partial protection from further degradation (as suggested by the reduction in oxidation rate over time), it also leads to formation of new surface defects that serve as efficient carrier traps. The formation of surface oxides and a partial loss of near-surface Se and Pb atoms are also responsible for the reduction of the effective NC core size and a corresponding increase in the energy gap. This is detected experimentally as a blue shift of the PL band and the spectral onset of absorption. In addition, the increase in E_g leads to reduction in the efficiency of "intrinsic" nonradiative recombination, which we identify as the main reason for the experimentally observed increase in the exciton lifetime (Figure 3b) and the recovery of the PL QY (Figure 2d). This model implies that the rate and the magnitude of the PL recovery depend on the rate and efficiency of two competing processes: enhancement of nonradiative surface carrier trapping, which reduces PL QY, and suppression of "intrinsic" nonradiative recombination, which enhances PL QY. In the case where the latter effect is dominant, the PL recovery is observed as a result of NC oxidation. In the case of a predominant role of additional carrier losses due to formation of new surface traps, the PL is irrecoverably quenched. The relative efficiency of the two processes is likely to be dictated by factors such as surface chemical composition (*e.g.*, Pb/Se ratio) and/or the quality and the type of surface passivation. These factors are expected to vary with the details of the NC synthesis and purification procedures.

CONCLUSIONS

We have shown that exposure of PbSe NCs in hexane solution to air at ambient conditions leads to rapid oxidation of PbSe, whereby PbO, SeO_2, and/or $PbSeO_3$ are formed on the NC surface. This process does not require activation by light absorption as it is thermally induced and spontaneous at room temperature. Oxidation reduces the size of the NCs (in some cases by more than ~50% of the volume) and increases their size dispersion, which leads to blue shifts and broadening of both the PL spectrum and the band-edge absorption feature. The short-term (minutes) drop in the PL QY,

detected in all samples immediately upon air exposure, is attributed to enhanced nonradiative carrier trapping induced by adsorption of oxygen onto the surfaces of NCs. Long-term (hours) recovery of the PL QY is attributed to a reduction in the rate of "intrinsic" nonradiative interband recombination caused by the increase in the energy gap in oxidized NCs. In samples in which the suppression of "intrinsic" nonradiative recombination is overwhelmed by the increase in nonradiative carrier losses due to trapping at surface defects, long-term PL recovery is not observed. A thin shell of CdSe formed on PbSe NCs *via* an ion exchange process provides good protection of the PbSe core from oxidation but does not completely isolate the carriers from defects formed on the surface of the shell as a result of long-term air exposure.

Studies of carrier relaxation dynamics have shown that the time scale for nonradiative carrier trapping associated with adsorption of oxygen and/or surface oxidation of NCs is comparable with Auger recombination and that the inherent dynamics of the Auger process is only weakly affected by the surface oxidation. Specifically, the Auger decay times following air exposure are changed only moderately (shortened by *ca.* 10−50%) compared to "air-free" NCs with the same energy gap. We also demonstrated that if the effect of carrier trapping observed in air exposed samples is not explicitly accounted for, the analysis of early-to-late time PL intensities leads to overestimation of CM efficiencies. Using a modified analysis, which corrects for the effect of trapping, we have shown that the dramatic changes in surface properties of PbSe NCs following air exposure and the development of competitive relaxation channels do not significantly affect the efficiency of the CM process.

While CM is not significantly affected by the exposure of NCs to air, the air-exposure-induced formation of new nonradiative relaxation channels is detrimental to application of PbSe NCs in light-emitting and lasing devices. The enhanced carrier relaxation and formation of oxides on the surfaces of NCs are also likely to serve as an impediment to efficient carrier extraction from photoexcited NCs, which is critical to solar energy conversion applications. Therefore, incorporation of PbSe NCs into practical lighting or solar energy conversion devices will likely require either use of strictly anaerobic conditions or development of approaches where the NCs are protected from the effects of air exposure by chemical means (*e.g.*, the core/shell approach studied here) or by incorporation of the NCs into protective matrices.

METHODS

Chemicals. Lead(II) oxide (PbO, Alfa Aesar, 99.9995%), trioctylphosphine (TOP, Strem, 97%), di-*i*-butylphosphine [$(i\text{-Bu})_2$PH, Strem, 98+%], selenium shot (Alfa Aesar, 99.999%), phenyl ether (Acros, 99%), anhydrous ethanol, hexane, and toluene were used without additional purification. A 2 M trioctylphosphine selenium (TOPSe) stock solution was prepared by heating an appropriate amount of TOP and selenium shot to 120 °C and stirring until dissolved. All syntheses were conducted under argon atmosphere by standard Schlenk or glovebox techniques.

Synthesis of 2.0 μm-Emitting PbSe NCs. The procedure used for the preparation of PbSe NCs is based on published high-chemical-yield methods[5] modified to completely avoid air exposure. A 0.2 g portion (0.9 mmol) of PbO, 1 mL (3 mmol) of oleic acid, 0.05 mL (0.3 mmol) of di-*i*-butylphosphine, 2 mL of phenyl ether, and 3 mL of TOP were loaded into a vial sealed with a silicone septum in a glovebox. The mixture was heated to 150 °C for 1.5 h under Ar flow delivered by a needle through the septum. After cooling, the vial was opened within a glovebox, and heated to 190 °C on a hot plate. Subsequently, 1.4 mL of 2 M solution of TOPSe in TOP was rapidly injected. The reaction was quenched after 10 s by immersing the vial in a larger beaker containing cold toluene while slowly adding ~8 mL hexane to the vial until rapid boiling stops. Then the NCs were precipitated by the addition of ethanol (*ca.* 7−10 mL). After the NC solids were collected by centrifugation and decanting, they were redispersed in hexane for further studies.

Synthesis of PbSe NCs of other sizes was accomplished by slight modifications of the above procedure. Smaller NCs were prepared using lower injection temperatures, shorter reaction times, and larger amounts of di-*i*-butylphosphine; larger dots were prepared by using higher injection temperatures and longer reaction times.

Synthesis of PbSe/CdSe NCs. PbSe NCs were prepared as described above and dispersed in toluene solution in a glovebox. Shell growth by cation exchange was then performed as described in a previous report,[6] with the slight refinement that anhydrous, degassed solvents were used during isolation of the NC solids, and redispersion and further handling were carried out in a glovebox.

Sample Treatment. Following synthesis, the NCs were stored in hexane in a glovebox under Ar atmosphere. For the studies of air-free samples, the NCs in hexane solution were transferred into quartz cuvettes with airtight seals. For the air-exposure experiments the NCs were transferred into quartz cuvettes without caps and removed from the glovebox. Between the physical measurements the cuvettes with NC solutions were typically stored in a 5 L desiccator open to external atmosphere at room temperature. Fresh anhydrous hexane was added to the NC solution whenever ~50% of the solvent had evaporated. For the low-temperature experiment, the NC solution was stored in a freezer at −35 °C.

Experimental Methods. Absorption spectra were collected using a Perkin-Elmer Lambda 1050 UV/vis/NIR spectrophotometer in the absorbance mode. The steady-state PL spectra for diluted NC samples in hexane were recorded with a liquid N_2 cooled InSb detector using an excitation wavelength of 808 nm. The excitation beam was mechanically chopped, and the signal was measured by a lock-in amplifier. The quantum efficiencies were calculated with respect to IR26 (Exciton) in 1,2-dichloroethane, and corrections were made to account for the grating and detector efficiencies. The QY of IR26 was assumed to be 0.50%.[34] Time-resolved (nanosecond) PL measurements were performed using a Hamamatsu H9170-75 NIR PMT detector with a time resolution of ~1 ns.

Picosecond PL measurements were performed using PL upconversion (uPL)[61] in which the sample was excited by 1.54 or 3.08 eV, 3 ps pulses from a frequency-doubled amplified Ti:sapphire laser and the emission was frequency-mixed (gated) with 1.55 eV, 3 ps pulses in a β-barium borate (β-BBO) nonlinear-optical crystal. The pulses from the laser were stretched to several picsoseconds to minimize the background in the upconversion signal arising from parametric down-conversion of intense gate pulses in the upconversion crystal. The sum frequency

signal was spectrally filtered with a monochromator and detected using a cooled photomultiplier tube coupled to a photon counting system. The time resolution of the uPL measurements was ~4 ps. All PL measurements were performed at room temperature. A more detailed description of the method is given elsewhere.[66]

X-ray photoelectron spectroscopy (XPS) measurements were performed using a Physical Electronics PHI 5600ci spectrometer system with monochromatic Al Kα (1486.6 eV) X-ray radiation. The base pressure during the measurements was on the order of 10^{-10} Torr. All XPS spectra were collected at 15 kV with X-ray power of 350 W, at a resolution of 23.5 eV, and at 45° angle relative to the sample plane on which the NCs were deposited. All spectra were charge-referenced to the carbon present as part of the ligand or as adventitious carbon at 285.0 eV binding energy.

For the air-free experiments, the NCs were deposited in a glovebox from solution by dropcasting onto a Si wafer, rinsed several times with anhydrous methanol, and transferred in a vacuum-tight sample holder into the XPS chamber. The air-exposed samples were deposited onto the Si substrate under ambient conditions, transferred to a glovebox where they were rinsed several times with anhydrous methanol, and subsequently transferred to a vacuum-tight sample holder and ultimately to the XPS chamber.

Curve fitting of the XPS spectra was performed using the PHI Multipak software package in order to identify and quantify the various metal component chemical states present at the surfaces of the NCs. Binding energies of the various fit component peaks were restricted to energies relevant for the chemical states present, ratios between spin−orbit split peaks were correctly maintained, peaks were 80% Gaussian and 20% Lorentzian, and peak widths were determined by the intrinsic broadening and analyzer resolution used, usually 1.2−1.4 eV fwhm.

The TEM measurements were performed using a JEOL-300 microscope with an accelerating voltage of 300 keV. The samples for TEM studies were prepared by dispersing the diluted NC solution on carbon-coated copper grids. For air-free experiments, the NCs were deposited on the grid and transferred into an air-tight sample container in a glovebox under Ar atmosphere. The samples were then transferred in the airtight container to the TEM chamber for analysis. During the transfer of the samples from the container to the TEM chamber they were air exposed for ~5 s.

Acknowledgment. M.S., A.Y.K., and J.A.M. acknowledge support by Los Alamos National Laboratory Directed Research and Development Funds. V.I.K. is supported by the Center for Advanced Solar Photophysics, an Energy Frontier Research Center funded by the U.S. Department of Energy (DOE), Office of Science, Office of Basic Energy Sciences (BES). J.M.P. and J.A.M acknowledge support by the Chemical Sciences, Biosciences and Geosciences Division of BES, U.S. DOE. We thank D. Werder for the assistance with the acquisition of the TEM images.

Supporting Information Available: The analysis of the uPL decays. This material is available free of charge *via* the Internet at http://pubs.acs.org.

REFERENCES AND NOTES

1. Murray, C. B.; Sun, S.; Gaschler, W.; Doyle, H.; Betley, T. A.; Kagan, C. R. Colloidal Synthesis of Nanocrystals and Nanocrystal Superlattices. *IBM. J. Res. Dev.* **2001**, *45*, 47–56.
2. Hui, D.; Chialing, C.; Krishnan, R.; Krauss, T. D.; Harbold, J. M.; Wise, F. W.; Thomas, M. G.; Silcox, J. Optical Properties of Colloidal PbSe Nanocrystals. *Nano Lett.* **2002**, *2*, 1321–1324.
3. Wehrenberg, B. L.; Wang, C. J.; Guyot-Sionnest, P. Interband and Intraband Optical Studies of PbSe Colloidal Quantum Dots. *J. Phys. Chem. B* **2002**, *106*, 10634–10640.
4. Hines, M. A.; Scholes, G. D. Colloidal PbS Nanocrystals with Size-Tunable Near-Infrared Emission: Observation of Post-Synthesis Self-Narrowing of the Particle Size Distribution. *Adv. Mater.* **2003**, *15*, 1844–1849.
5. Pietryga, J. M.; Schaller, R. D.; Werder, D.; Stewart, M. H.; Klimov, V. I.; Hollingsworth, J. A. Pushing the Band Gap Envelope: Mid-Infrared Emitting Colloidal PbSe Quantum Dots. *J. Am. Chem. Soc.* **2004**, *126*, 11752–11753.
6. Pietryga, J. M.; Werder, D. J.; Williams, D. J.; Casson, J. L.; Schaller, R. D.; Klimov, V. I.; Hollingsworth, J. A. Utilizing the Lability of Lead Selenide to Produce Heterostructured Nanocrystals with Bright, Stable Infrared Emission. *J. Am. Chem. Soc.* **2008**, *130*, 4879–4885.
7. Schaller, R. D.; Petruska, M. A.; Klimov, V. I. Tunable Near-Infrared Optical Gain and Amplified Spontaneous Emission Using PbSe Nanocrystals. *J. Phys. Chem. B* **2003**, *107*, 13765–13768.
8. Bakueva, L.; Musikhin, S.; Hines, M. A.; Chang, T. W. F.; Tzolov, M.; Scholes, G. D.; Sargent, E. H. Size-Tunable Infrared (1000−1600 nm) Electroluminescence from PbS Quantum-Dot Nanocrystals in a Semiconducting Polymer. *Appl. Phys. Lett.* **2003**, *82*, 2895–2897.
9. Steckel, J. S.; Coe-Sullivan, S.; Bulovic, V.; Bawendi, M. G. 1.3 to 1.55 μm Tunable Electroluminescence from PbSe Quantum Dots Embedded within an Organic Device. *Adv. Mater.* **2003**, *15*, 1862–1866.
10. Talapin, D. V.; Murray, C. B. Applied Physics: PbSe Nanocrystal Solids for n- and p-Channel Thin Film Field-Effect Transistors. *Science* **2005**, *310*, 86–89.
11. McDonald, S. A.; Konstantatos, G.; Zhang, S.; Cyr, P. W.; Klem, E. J. D.; Levina, L.; Sargent, E. H. Solution-Processed PbS Quantum Dot Infrared Photodetectors and Photovoltaics. *Nat. Mater.* **2005**, *4*, 138–142.
12. Xiaomei, J.; Schaller, R. D.; Lee, S. B.; Pietryga, J. M.; Klimov, V. I.; Zakhidov, A. A. PbSe Nanocrystal/Conducting Polymer Solar Cells with an Infrared Response to 2 Micron. *J. Mater. Res.* **2007**, *22*, 2204–2210.
13. Luther, J. M.; Law, M.; Beard, M. C.; Song, Q.; Reese, M. O.; Ellingson, R. J.; Nozik, A. J. Schottky Solar Cells Based on Colloidal Nancrystal Films. *Nano Lett.* **2008**, 5.
14. Sun, B.; Findikoglu, A. T.; Sykora, M.; Werder, D. J.; Klimov, V. I. Hybrid Photovoltaics Based on Semiconductor Nanocrystals and Amorphous Silicon. *Nano Lett.* **2009**, *9*, 1235–1241.
15. Luther, J. M.; Law, M.; Song, Q.; Perkins, C. L.; Beard, M. C.; Nozik, A. J. Structural, Optical, and Electrical Properties of Self-Assembled Films of PbSe Nanocrystals Treated with 1,2-Ethanedithiol. *ACS Nano* **2008**, *2*, 271–280.
16. Peterson, J. J.; Krauss, T. D. Photobrightening and Photodarkening in PbS Quantum Dots. *Phys. Chem. Chem. Phys.* **2006**, *8*, 3851–3856.
17. Stouwdam, J. W.; Shan, J.; Van Veggel, F. C. J. M.; Pattantyus-Abraham, A. G.; Young, J. F.; Raudsepp, M. Photostability of Colloidal PbSe and PbSe/PbS Core/Shell Nanocrystals in Solution and in the Solid State. *J. Phys. Chem. C* **2007**, *111*, 1086–1092.
18. Law, M.; Luther, J. M.; Song, Q.; Hughes, B. K.; Perkins, C. L.; Nozik, A. J. Structural, Optical and Electrical Properties of PbSe Nanocrystal Solids Treated Thermally or with Simple Amines. *J. Am. Chem. Soc.* **2008**, *130*, 5974–5985.
19. Dai, Q.; Wang, Y.; Zhang, Y.; Li, X.; Li, R.; Zou, B.; Seo, J.; Wang, Y.; Liu, M.; Yu, W. W. Stability Study of PbSe Semiconductor Nanocrystals over Concentration, Size, Atmosphere, and Light Exposure. *Langmuir* **2009**, *25*, 12320–12324.
20. Klimov, V. I.; Mikhailovsky, A. A.; Xu, S.; Malko, A.; Hollingsworth, J. A.; Leatherdale, C. A.; Eisler, H. J.; Bawendi, M. G. Optical Gain and Stimulated Emission in Nanocrystal Quantum Dots. *Science* **2000**, *290*, 314–317.
21. Klimov, V. I. Optical Nonlinearities and Ultrafast Carrier Dynamics in Semiconductor Nanocrystals. *J. Phys. Chem. B* **2000**, *104*, 6112–6123.
22. Schaller, R. D.; Klimov, V. I. High Efficiency Carrier Multiplication in PbSe Nanocrystals: Implications for Solar Energy Conversion. *Phys. Rev. Lett.* **2004**, *92*, 186601-1–186601-4.
23. Beard, M. C.; Knutsen, K. P.; Pingrong, Y.; Luther, J. M.; Qing, S.; Metzger, W. K.; Ellingson, R. J.; Nozik, A. J. Multiple Exciton Generation in Colloidal Silicon Nanocrystals. *Nano Lett.* **2007**, *7*, 2506–2512.

24. Ellingson, R. J.; Beard, M. C.; Johnson, J. C.; Yu, P.; Micic, O. I.; Nozik, A. J.; Shabaev, A.; Efros, A. L. Highly Efficient Multiple Exciton Generation in Colloidal PbSe and PbS Quantum Dots. *Nano Lett.* **2005**, *5*, 865–871.
25. Murphy, J. E.; Beard, M. C.; Norman, A. G.; Ahrenkiel, S. P.; Johnson, J. C.; Yu, P.; Micic, O. I.; Ellingson, R. J.; Nozik, A. J. PbTe Colloidal Nanocrystals: Synthesis, Characterization, and Multiple Exciton Generation. *J. Am. Chem. Soc.* **2006**, *128*, 3241–3247.
26. Minbiao, J.; Sungnam, P.; Connor, S. T.; Mokari, T.; Yi, C.; Gaffney, K. J. Efficient Multiple Exciton Generation Observed in Colloidal PbSe Quantum Dots with Temporally and Spectrally Resolved Intraband Excitation. *Nano Lett.* **2009**, *9*, 1217–1222.
27. Trinh, M. T.; Houtepen, A. J.; Schins, J. M.; Hanrath, T.; Piris, J.; Goossens, A. P. L. M.; Siebbeles, L. D. A. In Spite of Recent Doubts Carrier Multiplication Does Occur in PbSe Nanocrystals. *Nano Lett.* **2008**, *8*, 1713–1718.
28. McGuire, J. A.; Joo, J.; Pietryga, J. M.; Schaller, R. D.; Klimov, V. I. New Aspects of Carrier Multiplication in Semiconductor Nanocrystals. *Acc. Chem. Res.* **2008**, *41*, 1810–1819.
29. Kilina, S. V.; Kilin, D. S.; Prezhdo, O. V. Breaking the Phonon Bottleneck in PbSe and CdSe Quantum Dots: Time-Domain Density Functional Theory of Charge Carrier Relaxation. *ACS Nano* **2009**, *3*, 93–99.
30. Beard, M. C.; Midgett, A. G.; Law, M.; Semonin, O. E.; Ellingson, R. J.; Nozik, A. J. Variations in the Quantum Efficiency of Multiple Exciton Generation for a Series of Chemically Treated PbSe Nanocrystal Films. *Nano Lett.* **2009**, *9*, 836–845.
31. Guyot-Sionnest, P.; Wehrenberg, B.; Yu, D. Intraband Relaxation in CdSe Nanocrystals and the Strong Influence of the Surface Ligands. *J. Chem. Phys.* **2005**, 123.
32. Moreels, I.; Lambert, K.; De Muynck, D.; Vanhaecke, F.; Poelman, D.; Martins, J. C.; Allan, G.; Hens, Z. Composition and Size-Dependent Extinction Coefficient of Colloidal PbSe Quantum Dots. *Chem. Mater.* **2007**, *19*, 6101–6106.
33. Wehrenberg, B. L.; Congjun, W.; Guyot-Sionnest, P. Interband and Intraband Optical Studies of PbSe Colloidal Quantum Dots. *J. Phys. Chem. B* **2002**, *106*, 10634–10640.
34. Although the value of PL QY = 0.50% for IR26 dye used here is consistent with the literature (ref 33) the error associated with this value is unknown. As a result the PL QYs of PbSe NC solutions, measured here with IR26 as a reference, have also unknown associated errors. Therefore the PL QYs are presented as relative values.
35. We noticed that the NC chemical yield was significantly higher if the initial synthesis step was performed under static argon atmosphere. This points to an active role of di-*i*-butylphosphine in the formation of the NCs; di-*i*-butylphosphine also likely affects the chemical composition of the NC surface.
36. Battino, R.; Rettich, T. R.; Tominaga, T. The Solubility of Oxygen and Ozone in Liquids. *J. Phys. Chem. Ref. Data* **1983**, *12*, 163–178.
37. Dias, A. M. A.; Bonifacio, R. P.; Marrucho, I. M.; Padua, A. A. H.; Gomes, M. F. C. Solubility of Oxygen in *n*-Hexane and in *n*-Perfluorohexane. Experimental Determination and Prediction by Molecular Simulation. *Phys. Chem. Chem. Phys.* **2003**, *5*, 543–549.
38. Kigel, A.; Brumer, M.; Maikov, G.; Sashchiuk, A.; Lifshitz, E. The Ground-State Exciton Lifetime of PbSe Nanocrystal Quantum Dots. *Superlattices Microstruct.* **2005**, *46*, 272–276.
39. Moreels, I.; Lambert, K.; Smeets, D.; De Muynck, D.; Nollet, T.; Martins, J. C.; Vanhaecke, F.; Vantomme, A.; Delerue, C.; Allan, G.; *et al*. Size-Dependent Optical Properties of Colloidal PbS Quantum Dots. *ACS Nano* **2009**, *3*, 3023–3030.
40. Warner, J. H.; Thomsen, E.; Watt, A. R.; Heckenberg, N. R.; Rubinsztein-Dunlop, H. Time-Resolved Photoluminescence Spectroscopy of Ligand-Capped PbS Nanocrystals. *Nanotechnology* **2005**, *16*, 175–179.
41. Efros, A. L.; Rodina, A. V. Band-Edge Absorption and Luminescence of Nonspherical Nanometer-Size Crystals. *Phys. Rev. B* **1993**, *47*, 10005–10007.
42. Schaller, R. D.; Pietryga, J. M.; Goupalov, S. V.; Petruska, M. A.; Ivanov, S. A.; Klimov, V. I. Breaking the Phonon Bottleneck in Semiconductor Nanocrystals *via* Multiphonon Emission Induced by Intrinsic Nonadiabatic Interactions. *Phys. Rev. Lett.* **2005**, *95*, 1–4.
43. Ridley, B. K. *Electrons and Phonons in Semiconductor Multilayers*; Cambridge University Press: Cambridge, U.K., 2009.
44. Englman, R.; Jortner, J. The Energy Gap Law for Radiationless Transitions in Large Molecules. *Mol. Phys.* **1970**, *18*, 145–164.
45. Lansberg, P. *Recombination in Semiconductors*; University Press: Cambridge U.K., 1991.
46. Gautier, C.; Cambon-Muller, M.; Averous, M. Study of PbSe Layer Oxidation and Oxide Dissolution. *Appl. Surf. Sci.* **1999**, *141*, 157–163.
47. Sarkar, S. K.; Kababya, S.; Vega, S.; Cohen, H.; Woicik, J. C.; Frenkel, A. I.; Hodes, G. Effects of Solution pH and Surface Chemistry on the Postdeposition Growth of Chemical Bath Deposited PbSe Nanocrystalline Films. *Chem. Mater.* **2007**, *19*, 879–888.
48. Sameer, S.; Nanda, J.; Pietryga, J. M.; Hollingsworth, J. A.; Sarma, D. D. Unraveling Internal Structures of Highly Luminescent PbSe Nanocrystallites Using Variable-Energy Synchrotron Radiation Photoelectron Spectroscopy. *J. Phys. Chem. B* **2006**, *110*, 15244–15250.
49. Moreels, I.; Fritzinger, B.; Martins, J. C.; Hens, Z. Surface Chemistry of Colloidal PbSe Nanocrystals. *J. Am. Chem. Soc.* **2008**, *130*, 15081–15086.
50. In our TEM studies we have attempted to image the oxide shell on the surface of NCs. However, even with careful high resolution imaging we were unsuccessful. This could be for several reasons. The oxide shell is likely an amorphous material that may be hard to image due to insufficient contrast against the background. Alternatively, it is possible that a significant amount of shell material is lost from the surface while in solution or during the TEM sample preparation. With the experimental methods used in our studies we were unable to distinguish between these two possibilities.
51. Tomaev, V. V.; Makarov, L. L.; Tikhonov, P. A.; Solomennikov, A. A. Oxidation Kinetics of Lead Selenide. *Glass Phys. Chem.* **2004**, *30*, 349–355.
52. Popovkin, B. A.; Kovba, L. M.; Zlomanov, V. P.; Novoselova, A. V. An Investigation of the Reaction between Lead Selenide and Oxygen. *Dokl. Acad. Nauk SSSR* **1959**, *129*, 809–812.
53. Zlomanov, V. P.; Novoselova, A. V. Investigation of Interaction of Lead Selenide with Oxygen. *Dokl. Acad. Nauk SSSR* **1962**, *143*, 115.
54. Although Se_2 was not detected in the present study, XPS signatures of neutral Se were detected in our previous synchrotron study of strongly oxidized PbSe NCs.
55. Katari, J. E. B.; Colvin, V. L.; Alivisatos, A. P. X-ray Photoelectron Spectroscopy of CdSe Nanocrystals with Applications to Studies of the Nanocrystal Surface. *J. Phys. Chem.* **1994**, *98*, 4109–4117.
56. Aldana, J.; Wang, Y. A.; Peng, X. G. Photochemical Instability of CdSe Nanocrystals Coated by Hydrophilic Thiols. *J. Am. Chem. Soc.* **2001**, *123*, 8844–8850.
57. Javier, A.; Strouse, G. F. Activated and Intermittent Photoluminescence in Thin CdSe Quantum Dot Films. *Chem. Phys. Lett.* **2004**, *391*, 60–63.
58. van Sark, W.; Frederix, P.; Bol, A. A.; Gerritsen, H. C.; Meijerink, A. Blueing, Bleaching, and Blinking of Single CdSe/ZnS Quantum Dots. *Chem. Phys. Phys. Chem.* **2002**, *3*, 871–879.
59. Klimov, V. I.; McBranch, D. W.; Leatherdale, C. A.; Bawendi, M. G. Electron and Hole Relaxation Pathways in Semiconductor Quantum Dots. *Phys. Rev. B* **1999**, *60*, 13740–13749.

60. Nozik, A. J. Quantum Dot Solar Cells. *Phys. E* **2002**, *14*, 115–120.
61. Shah, J. Ultrafast Luminescence Spectroscopy Using Sum Frequency Generation. *IEEE J. Quant. Electr.* **1988**, *24*, 276–288.
62. Hanna, M. C.; Nozik, A. J. Solar Conversion Efficiency of Photovoltaic and Photoelectrolysis Cells with Carrier Multiplication Absorbers. *J. Appl. Phys.* **2006**, *100*, 1–8.
63. Klimov, V. I. Detailed-Balance Power Conversion Limits of Nanocrystal-Quantum-Dot Solar Cells in the Presence of Carrier Multiplication. *Appl. Phys. Lett.* **2006**, 89.
64. Schaller, R. D.; Sykora, M.; Jeong, S.; Klimov, V. I. High-Efficiency Carrier Multiplication and Ultrafast Charge Separation in Semiconductor Nanocrystals Studied *via* Time-Resolved Photoluminescence. *J. Phys. Chem. B* **2006**, *110*, 25332–25338.
65. Meincke, H.; Ebling, D. G.; Heinze, J.; Tacke, M.; Boettner, H. Potentiostatic Oxide Formation on Lead Selenide Single Crystals in Alkaline Solutions. *J. Electrochem. Soc.* **1998**, *145*, 2806–2812.
66. McGuire, J. A.; Sykora, M.; Joo, J.; Pietryga, J. M.; Klimov, V. I., Apparent *versus* True Carrier Multiplication Yields in Semiconductor Nanocrystals. Submitted for publication.